



HAL
open science

An α II Spectrin-Based Cytoskeleton Protects Large-Diameter Myelinated Axons from Degeneration

Claire Yu-Mei Huang, Chuansheng Zhang, Daniel Zollinger, Christophe Leterrier, Matthew Rasband

► **To cite this version:**

Claire Yu-Mei Huang, Chuansheng Zhang, Daniel Zollinger, Christophe Leterrier, Matthew Rasband. An α II Spectrin-Based Cytoskeleton Protects Large-Diameter Myelinated Axons from Degeneration. *Journal of Neuroscience*, 2017, 37 (47), pp.11323 - 11334. 10.1523/jneurosci.2113-17.2017 . hal-01701371

HAL Id: hal-01701371

<https://hal.science/hal-01701371>

Submitted on 13 Jul 2018

HAL is a multi-disciplinary open access archive for the deposit and dissemination of scientific research documents, whether they are published or not. The documents may come from teaching and research institutions in France or abroad, or from public or private research centers.

L'archive ouverte pluridisciplinaire **HAL**, est destinée au dépôt et à la diffusion de documents scientifiques de niveau recherche, publiés ou non, émanant des établissements d'enseignement et de recherche français ou étrangers, des laboratoires publics ou privés.

An α II Spectrin-Based Cytoskeleton Protects Large-Diameter Myelinated Axons from Degeneration

Claire Yu-Mei Huang,¹ Chuansheng Zhang,¹ Daniel R. Zollinger,¹  Christophe Leterrier,² and  Matthew N. Rasband¹

¹Department of Neuroscience, Baylor College of Medicine, Houston, Texas 77030, and ²NeuroCyto, NICN UMR7259, Aix Marseille Université, CNRS, 13344 cedex 15, Marseille, France

Axons must withstand mechanical forces, including tension, torsion, and compression. Spectrins and actin form a periodic cytoskeleton proposed to protect axons against these forces. However, because spectrins also participate in assembly of axon initial segments (AISs) and nodes of Ranvier, it is difficult to uncouple their roles in maintaining axon integrity from their functions at AIS and nodes. To overcome this problem and to determine the importance of spectrin cytoskeletons for axon integrity, we generated mice with α II spectrin-deficient peripheral sensory neurons. The axons of these neurons are very long and exposed to the mechanical forces associated with limb movement; most lack an AIS, and some are unmyelinated and have no nodes. We analyzed α II spectrin-deficient mice of both sexes and found that, in myelinated axons, α II spectrin forms a periodic cytoskeleton with β IV and β II spectrin at nodes of Ranvier and paranodes, respectively, but that loss of α II spectrin disrupts this organization. *Avil-cre;Sptan1^{fl/fl}* mice have reduced numbers of nodes, disrupted paranodal junctions, and mislocalized Kv1 K⁺ channels. We show that the density of nodal β IV spectrin is constant among axons, but the density of nodal α II spectrin increases with axon diameter. Remarkably, *Avil-cre;Sptan1^{fl/fl}* mice have intact nociception and small-diameter axons, but severe ataxia due to preferential degeneration of large-diameter myelinated axons. Our results suggest that nodal α II spectrin helps resist the mechanical forces experienced by large-diameter axons, and that α II spectrin-dependent cytoskeletons are also required for assembly of nodes of Ranvier.

Key words: axon; cytoskeleton; degeneration; node of Ranvier; spectrin

Significance Statement

A periodic axonal cytoskeleton consisting of actin and spectrin has been proposed to help axons resist the mechanical forces to which they are exposed (e.g., compression, torsion, and stretch). However, until now, no vertebrate animal model has tested the requirement of the spectrin cytoskeleton in maintenance of axon integrity. We demonstrate the role of the periodic spectrin-dependent cytoskeleton in axons and show that loss of α II spectrin from PNS axons causes preferential degeneration of large-diameter myelinated axons. We show that nodal α II spectrin is found at greater densities in large-diameter myelinated axons, suggesting that nodes are particularly vulnerable domains requiring a specialized cytoskeleton to protect against axon degeneration.

Introduction

Axons connect neurons with their targets. These targets may be located far away, sometimes thousands of times the diameter of the soma. These distances are challenging because axons must

traffic proteins to and from nerve terminals, propagate action potentials rapidly and efficiently, and maintain structural integrity despite exposure to disruptive mechanical forces. The axon's submembranous cytoskeleton is organized into repeating circumferential actin rings evenly spaced and connected to one another by spectrins (Xu et al., 2013). This remarkable organization may render axons strong and flexible, allowing them to withstand compression, tension, and torsion resulting from, for example, the bending of a limb. Consistent with this idea, the axons of β spectrin-deficient worms are fragile and easily break. However, axons remain intact in paralyzed worms, suggesting that spectrin cytoskeletons help protect axons from the mechanical stresses associated with movement (Hammarlund et al., 2007; Krieg et al., 2017).

Received July 26, 2017; revised Sept. 11, 2017; accepted Oct. 4, 2017.

Author contributions: C.Y.-M.H. and M.N.R. designed research; C.Y.-M.H., C.Z., D.R.Z., C.L., and M.N.R. performed research; C.Y.-M.H., D.R.Z., C.L., and M.N.R. analyzed data; C.Y.-M.H. and M.N.R. wrote the paper.

This work was supported by National Institutes of Health Grants NS044916 and NS069688 to M.N.R., and the Dr. Miriam and Sheldon G. Adelson Medical Research Foundation. C.L. acknowledges Dr. Benedicte Dargent for support. We thank Dr. Marie-Pierre Blanchard for help with STORM imaging.

The authors declare no competing financial interests.

Correspondence should be addressed to Dr. Matthew N. Rasband, Department of Neuroscience, Baylor College of Medicine, One Baylor Plaza, Houston, TX 77030. E-mail: rasband@bcm.edu.

DOI:10.1523/JNEUROSCI.2113-17.2017

Copyright © 2017 the authors 0270-6474/17/3711323-12\$15.00/0

Spectrins function as tetramers consisting of two α and two β subunits (Bennett and Lorenzo, 2013). In vertebrate axons, α II spectrin is the only α spectrin and partners mainly with β I, β II, and β IV spectrin (Berghs et al., 2000; Ogawa et al., 2006; Ho et al., 2014; Zhang et al., 2014). Although α II spectrin is found throughout the axon, it may be enriched in specialized domains where specific β spectrins play distinct roles. For example, α II and β IV spectrin form a complex with ankyrinG (ankG) at axon initial segments (AISs) where these cytoskeletal proteins help cluster Na^+ channels (Berghs et al., 2000; Yang et al., 2007; Huang et al., 2017). In addition, α II and β II spectrin form a complex at paranodal junctions of myelinated axons where they assemble a cytoskeletal boundary that restricts Na^+ and K^+ channels to nodes and juxtaparanodes, respectively (Zhang et al., 2013; Amor et al., 2017). In zebrafish, α II spectrin is transiently detected at developing nodes of Ranvier where it contributes to node assembly. However, α II spectrin-deficient mice and zebrafish are embryonic and larval lethal, respectively, precluding any analysis of the role of α II spectrin's function in axon maintenance (Voas et al., 2007; Stankewich et al., 2011). Furthermore, axon injury and degeneration may result from disruption of the spectrin cytoskeleton because spectrins are proteolyzed by the Ca^{2+} -dependent protease calpain (Siman et al., 1984; Schafer et al., 2009).

To circumvent embryonic lethality and to determine the function of α II spectrin-dependent axonal cytoskeletons in (1) axon integrity, and (2) assembly of nodes, paranodes, and juxtaparanodes, we generated *Avil-cre;Sptan1^{fl/fl}* mice lacking neuronal α II spectrin in peripheral sensory neurons. We found that the α II spectrin-dependent cytoskeleton is dispensable for maintenance of small-diameter axons but is required for axon integrity in large-diameter myelinated axons. Furthermore, we found that α II spectrin forms a periodic cytoskeleton at nodes and paranodes in mammalian myelinated axons and is required for node of Ranvier assembly and maintenance. Our results suggest that nodal α II spectrin protects large-diameter axons from injury and degeneration.

Materials and Methods

Animals. To generate a conditional allele for *Sptan1*, a targeting vector was designed to replace an 8.5 kb genomic fragment with loxP sites flanking exon 8 of *Sptan1*. This targeting vector construct was electroporated into embryonic stem cells derived from 129/Sv mice. Colonies were selected and screened by Southern blot. Embryonic stem cells with correct homologous recombinations were injected into blastocysts and then transferred to foster female mice. Chimeric mice were crossed with C57BL/6 mice to confirm germline transmission. Upon crossing with cre recombinase-expressing mice, exon 8 will be excised and results in the premature termination of the *Sptan1* transcript. *Sptan1^{fl/fl}* mice were crossed with *CNP-cre* and *Advillin-cre (Avil-cre)* mice to spatially eliminate α II-spectrin in Schwann cells and DRG neurons, respectively. The *Sptan1^{fl/fl}* mice were maintained on a 129/Sv and C57BL/6 mixed background. All experiments involving animals complied with National Institutes of Health guidelines and were approved by the Animal Care and Use Committee at Baylor College of Medicine. PCR genotyping of mice was performed using the following primers: floxed *Sptan1*: forward, 5'-AACAGTCACACCCTCTGAGTGCCA-3'; reverse, 5'-ATTCAGTGGAAAGCTGAGAAG CCAG; *Avil-cre*: primer 1 (Avil/003F)-5'-CCCTGTTCAGTGTGAGTAGG; primer 2 (Avil/002B)-5'-AGTATCTGGTAGGTCCTCCAG-3'; primer 3 (Cre/001B)-5'-GCGATCCCTGAACATGTCATC-3'.

Intravitreal injection with adeno-associated virus (AAV) virus and analysis on optic nerve. To remove α II-spectrin in optic nerves, 3-month-old *Sptan1^{fl/fl}* mice were subjected to intravitreal injection with an AAV (Vector Biolabs; AAV2, 10^{12} GC/ml, 1:2 dilution in sterilized PBS) ex-

pressing Cre recombinase with GFP reporter. A virus expressing GFP (AAV-GFP) alone was used as control. One month after injection, optic nerves were dissected and analyzed by immunofluorescence labeling of GFP and nodal proteins.

Antibodies. The following primary antibodies were used: mouse monoclonal antibodies to α II-spectrin (clone D8B7, Biolegend; RRID: AB_2564660), β II-spectrin (BD Bioscience; RRID:AB_399853), Tuj1 (Biolegend; RRID:AB_2313773), and S46 (Developmental Studies Hybridoma Bank; RRID:AB_528376). ankG (N106/36; RRID:AB_10673030), Caspr (K65/35; RRID:AB_10806491), Kv β 2 (K17/70; RRID:AB_2131373), and Kv1.2 (K14/16; RRID:AB_2296313) antibodies were purchased from the University of California at Davis/National Institutes of Health NeuroMab Facility (Davis, CA). The pan- Na^+ channel monoclonal antibody (K58/35; RRID:AB_477552) was generated against a peptide containing the sequence TEEQKKYYNAMKGLGSKK, a highly conserved segment of the intracellular III-IV loop. Rabbit polyclonal antibodies were as follows: neurofilament M (EMD Millipore; RRID:AB_91201), GFP (A-11122, Thermo Fisher Scientific; RRID:AB_221569), ATF3 (Santa Cruz Biotechnology; RRID:AB_2258513), 4.1B (generated against a fusion protein containing amino acids 778–968 of human 4.1B was a gift from Dr. Elior Peles, Weizmann Institute of Science), and β IV spectrin (generated against the peptide sequence DRAEELPRRRRPERQE found in the C-terminal “specific domain”; RRID:AB_2315634). Chicken polyclonal antibody against neurofascin (AF3235; RRID:AB_10890736) was purchased from R&D Systems and goat polyclonal antibodies against Contactin (RRID:AB_2044647) were obtained from Santa Cruz Biotechnology and R&D Systems, respectively. Secondary antibodies AlexaFluor-350, -488, -594, and -647 were purchased from Thermo Fisher Scientific.

Immunofluorescence microscopy and STochastic Optical Reconstruction Microscopy (STORM) imaging. For immunostaining of nervous system tissues, nerves were collected at the indicated time points, fixed in 4% PFA on ice for 1 h. For the other tissues, muscles, skin, and cornea were also fixed in 4% PFA but for 2 h, overnight, and 1 h, respectively. The fixed tissues were then immersed in 20% sucrose in 0.1 M phosphate buffer overnight at 4°C. After this, tissues were embedded in OCT compound (Tissue-Tek #4583) and then sectioned using a cryostat (Thermo Scientific, Cryostar NX70) on glass coverslips for immunostaining. Procedures for immunofluorescence labeling were performed as previously described (Ogawa et al., 2006). Images of immunofluorescence were captured using an Axio-imager Z1 microscope (Carl Zeiss MicroImaging) or Axio-observer Z1 microscope (Carl Zeiss MicroImaging) fitted with an AxioCam digital camera (Carl Zeiss MicroImaging). Images were taken using 20 \times (0.8 NA), 40 \times (1.0 NA), 40 \times (0.75 NA), or 63 \times (1.4 NA) objectives. Images were then collected by Zen (Carl Zeiss MicroImaging) acquisition software. Measurement of fluorescence intensity was performed using FIJI (National Institutes of Health) and Zen. Measurement of DRG neuron diameter was performed in FIJI after immunostaining using antibodies against Kv β 2. In some cases, Z stacks and 3D reconstructions were performed using Zen. In some instances, STORM imaging was performed on an N-STORM microscope (Nikon Instruments). Coverslips were imaged in STORM buffer: 50 mM Tris, pH 8, 10 mM NaCl, 10% glucose, 100 mM MEA, 3.5 U/ml pyranose oxidase, and 40 mg/ml catalase. The samples were continuously illuminated at 647 nm (full power), and 30,000–60,000 images were acquired at 67 Hz, with progressive reactivation by simultaneous 405 nm illumination (Leterrier et al., 2015).

Transmission electron microscopy (TEM). Animals were perfused with 2.5% glutaraldehyde and 2.0% PFA in 0.1 M cacodylate buffer, pH 7.4. Dorsal roots were dissected and postfixed in the same fixative for overnight. The tissues were then postfixed in 1% osmium tetroxide solution in 0.1 M cacodylate buffer, pH 7.4, for 1 h. After washing, nerves went through a series of gradual dehydration by increasing percentage of ethanol (50%, 70%, 95%, and 100%) and gradually infiltrated with increasing percentage of Spurr's resin (Electron Microscopy Sciences). After infiltration, the tissues were then embedded in pure resin. Cross and longitudinal sections were cut and stained with Toluidine blue and staining for TEM. The sectioning and electron microscopy were performed in the Baylor College of Medicine Integrated Microscopy Core using a Hitachi H-7500 TEM.

Behavior. Gait analysis: The hindpaws of mice were dipped in ink so that the footprints were left on the lining of paper as they walked along a track to a dark goal box. **Wire-hang test:** Mice were placed on a wire net, which was then inverted and suspended above the home cage. The latency to fall was recorded. Three trials were performed for each animal, and the time of the trial that the mouse lasted longest was recorded. The cutoff time was set at 3 min. Mice received were given a latency of 180 s if they did not fall within 3 min trial period. **Tail immersion test:** Mice were held in the rodent holder with exposed tails; 2 cm of tail was then dipped in 50°C hot water. The time until the mouse flicked its tail was recorded.

Compound action potential (CAP) recording. CAP recordings were performed as described previously (Susuki et al., 2013). Briefly, dorsal roots were dissected and immediately placed in a continuously perfused recording chamber. Both ends of the root were drawn into suction electrodes, and the responses to a depolarizing current were recorded. Nerve conduction was calculated by dividing the length of the root by the time from stimulation to the peak of the CAP.

Statistics. No statistical methods were used to predetermine sample sizes, but our sample sizes are similar to those reported previously (Susuki et al., 2013). All statistical analyses were performed using GraphPad Prism software or Microsoft Excel. Error bars indicate SEM. Unpaired, two-tailed Student's *t* test was used for statistical analyses unless otherwise specified. Except for electrophysiology, data collection and analyses were not performed blindly to the conditions of the experiments. Data distribution was assumed to be normal.

Results

Loss of α II spectrin from peripheral sensory neurons causes sensorimotor dysfunction

We previously generated mice lacking only CNS α II spectrin (Huang et al., 2017). These mice have dramatic reductions in β spectrins, making the *Sptan1^{fl/fl}* mice a powerful tool to study the importance of submembranous spectrin cytoskeletons in nervous system function. *Nestin-cre;Sptan1^{fl/fl}* mice have widespread axon degeneration, disrupted AIS, and seizures and die within 3 weeks of birth. However, because AISs are responsible for both action potential initiation and maintenance of neuronal polarity (Rasband, 2010), it is not possible to determine whether axon degeneration results from disrupted AIS or loss of the spectrin cytoskeleton throughout the axon. Furthermore, α II spectrin has not been reported at mammalian nodes of Ranvier, and its role in node assembly in mammals remains unknown. To determine the importance and role of the spectrin cytoskeleton in supporting long axons and to uncouple the role of the AIS spectrin cytoskeleton from its function in distal axons, we crossed *Sptan1^{fl/fl}* mice with *Avil-cre* mice to generate mice lacking α II spectrin in peripheral sensory neurons. *Avil-cre* mice undergo recombination in sensory neurons beginning at E12.5 (Hasegawa et al., 2007). Immunostaining of dorsal roots from *Sptan1^{fl/fl}* showed α II spectrin immunoreactivity in both axons and Schwann cells (Fig. 1*a*). To reveal the axonal α II spectrin, we generated *CNP-cre;Sptan1^{fl/fl}* mice, which lack α II spectrin in Schwann cells (Fig. 1*a*). In contrast, *Avil-cre;Sptan1^{fl/fl}* mice showed α II spectrin in myelinating Schwann cells, but not axons (Fig. 1*a*), and the α II spectrin staining was much weaker in Schwann cells than axons. Finally, we confirmed the complete loss of α II spectrin in dorsal roots from *CNP-cre;Avil-cre;Sptan1^{fl/fl}* mice (Fig. 1*a*). Thus, *Avil-cre;Sptan1^{fl/fl}* mice lack α II spectrin in dorsal root axons.

To determine the function of α II spectrin in axons, we focused on *Avil-cre;Sptan1^{fl/fl}* mice. We found that these mice had a prominent hindlimb clasping reflex (Fig. 1*b*), severe ataxia (Fig. 1*c*), and dramatically impaired performance on the Wire-hang test (Fig. 1*d*). Surprisingly, when we measured nociception by the tail immersion assay, we found no difference between *Sptan1^{fl/fl}* and

Avil-cre;Sptan1^{fl/fl} mice (Fig. 1*e*). To determine whether loss of α II spectrin affects the functional properties of sensory axons, we measured the CAP in dorsal roots and calculated the peak conduction velocity corresponding to the fastest-conducting large-diameter myelinated axons. Sensory roots lacking α II spectrin had a 50% reduction in the CAP conduction velocity and reduced CAP amplitude (Fig. 1*f,g*). Together, these results suggest that myelinated sensory axons (e.g., proprioceptors and mechanoreceptors) may be preferentially affected by loss of α II spectrin.

α II spectrin forms a periodic cytoskeleton in PNS nodes of Ranvier

Myelinated axons have an α II spectrin/ β II spectrin-based paranodal cytoskeleton that functions as a lateral diffusion barrier to facilitate the assembly of nodes of Ranvier (Garcia-Fresco et al., 2006; Ogawa et al., 2006; Amor et al., 2017). However, because nodes and AIS share a common molecular organization (Chang and Rasband, 2013), we considered whether α II spectrin might also be found at nodes of Ranvier and participate in their assembly and maintenance. Previous studies in zebrafish had shown a transient localization of α II spectrin to nodes of Ranvier during early development, suggesting a role for α II spectrin in early node development (Voas et al., 2007). We immunostained detergent extracted and teased myelinated axons from adult sciatic nerve using antibodies against α II spectrin, protein 4.1b (protein 4.1b links β II spectrin to the paranodal axonal cell adhesion molecule Caspr (Poliak et al., 2001), and neurofascin (Nfasc). In addition to the previously reported paranodal α II spectrin, we found nodal α II spectrin that was flanked by protein 4.1b and that colocalized with nodal Nfasc (Fig. 2*a*, arrow). To determine the organization of the nodal spectrin cytoskeleton, we performed STORM imaging on nodes from teased dorsal root myelinated axons. These experiments revealed prominent nodal and paranodal α II spectrin organized as a periodic cytoskeleton with a spacing of \sim 190 nm in control myelinated axons (Fig. 2*b–e*). Similarly, and consistent with previous reports (D'Este et al., 2017), nodal β IV spectrin is also organized into a periodic cytoskeleton (Fig. 2*j–m*). In contrast, β II spectrin is excluded from nodes but still found in a periodic arrangement in paranodal and juxtaparanodal domains (Fig. 2*r–u*). STORM imaging of *Avil-cre;Sptan1^{fl/fl}* mice using antibodies against α II spectrin confirmed the specificity of the antibodies we used (Fig. 2*f–i*). More importantly, STORM imaging of *Avil-cre;Sptan1^{fl/fl}* mice using antibodies against β IV spectrin (Fig. 2*n–q*) and β II spectrin (Fig. 2*v–y*) showed that the periodic organization of nodal β IV spectrin and paranodal β II spectrin was completely disrupted. Thus, α II spectrin is required for the proper organization of the nodal and paranodal submembranous cytoskeleton.

Loss of α II spectrin disrupts node of Ranvier assembly

In addition to disruption of the periodic cytoskeleton, what consequences does loss of α II spectrin have for nodes of Ranvier? Previous studies using a mutant zebrafish lacking α II spectrin showed that loss of α II spectrin resulted in fragmented nodal Na⁺ channel clusters (Voas et al., 2007). We extended these observations by immunostaining dorsal roots throughout development and in adults to show that, whereas *Sptan1^{fl/fl}* dorsal roots have many nodes (Fig. 3*a*), with well-defined nodal, paranodal, and juxtaparanodal membrane domains (Fig. 3*a,b*), *Avil-cre;Sptan1^{fl/fl}* mice had significantly fewer intact nodes of Ranvier (Fig. 3*c,e*), frequent heminodes (Fig. 3*c*, arrows), and Kv1.2-containing K⁺ channels were no longer restricted to juxtaparan-

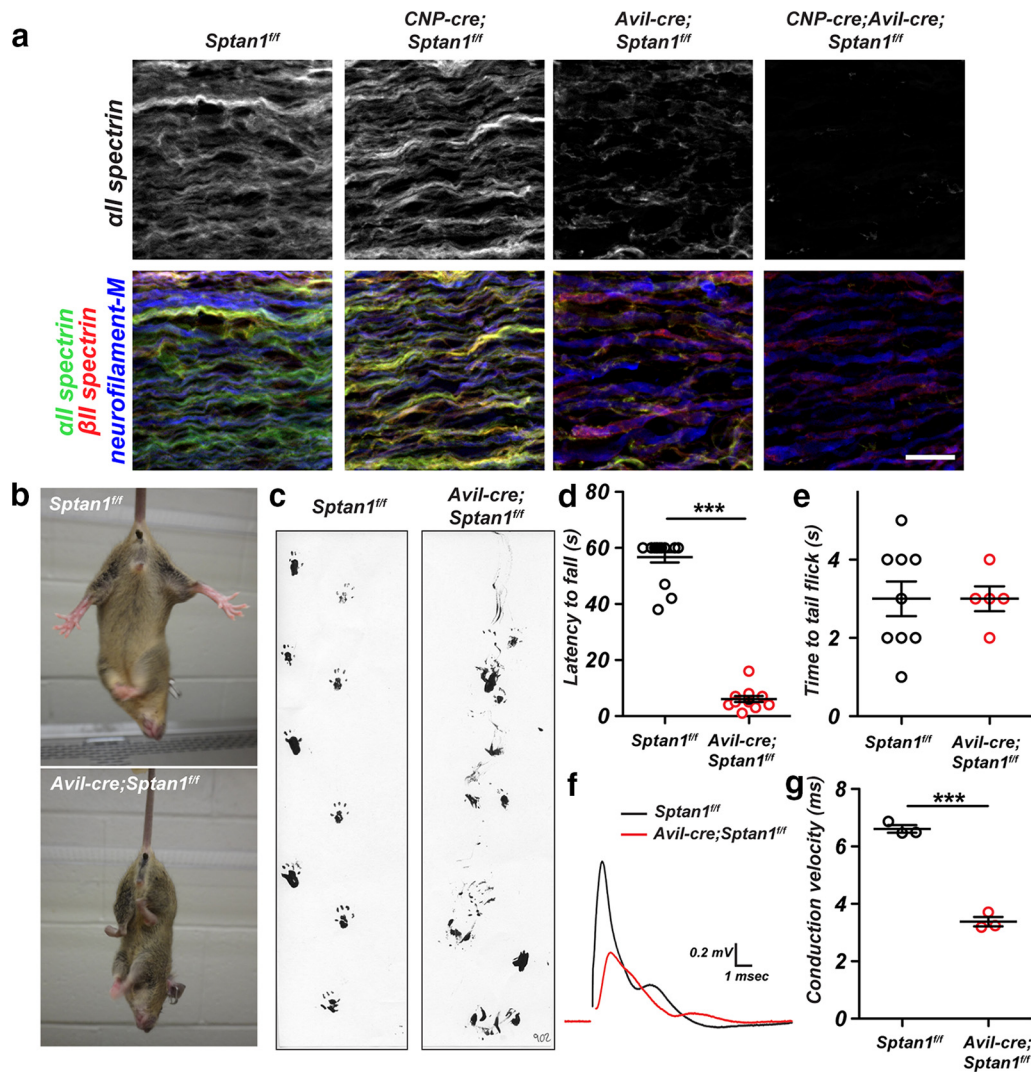


Figure 1. Sensory neuron-specific deletion of α II spectrin. **a**, Teased dorsal roots of P14 *Sptan1^{fl/fl}*, *CNP-cre;Sptan1^{fl/fl}*, *Avil-cre;Sptan1^{fl/fl}*, and *CNP-cre;Avil-cre;Sptan1^{fl/fl}* mice immunostained with antibodies against α II spectrin (green), β II spectrin (red), and neurofilament-M (blue). Scale bar, 20 μ m. **b**, *Avil-cre;Sptan1^{fl/fl}* mice show a hind-limb clasping reflex. **c**, Footprint assay for 1-month-old *Sptan1^{fl/fl}* and *Avil-cre;Sptan1^{fl/fl}* mice. **d**, Wirehang test performed on 1-month-old mice. *Sptan1^{fl/fl}*, $N = 16$; *Avil-cre;Sptan1^{fl/fl}*, $N = 12$. Data are mean \pm SEM. *** $p = 2.808 \times 10^{-18}$, $t_{(26)} = 21.90$. **e**, Tail immersion test performed on 1-month-old mice. *Sptan1^{fl/fl}*, $N = 9$; *Avil-cre;Sptan1^{fl/fl}*, $N = 5$. Data are mean \pm SEM. **f**, Representative CAPs recorded from 1-month-old *Sptan1^{fl/fl}* (black) and *Avil-cre;Sptan1^{fl/fl}* (red) dorsal roots. **g**, Conduction velocities recorded from dorsal roots of 1-month-old mice. *Sptan1^{fl/fl}*, $N = 3$ mice, 14 dorsal roots; *Avil-cre;Sptan1^{fl/fl}*, $N = 3$ mice, 15 dorsal roots. Data are mean \pm SEM. *** $p = 0.0001$, $t_{(4)} = 15.33$.

odal domains but could even be found throughout the node (Fig. 3*d*, arrow). Nodes across all fiber diameters were affected by the loss of α II spectrin. Measurement of nodal Na^+ channel fluorescence intensity showed a significant reduction compared with controls in mice older than 2 weeks of age (Fig. 3*f*), indicating an important role for α II spectrin in maintenance of Na^+ channel density. At all ages examined, immunostaining using antibodies against Caspr revealed dramatic disruption of paranodes (Fig. 3*g*), and an accompanying reduction in the number of nodes flanked by clustered K^+ channels (Fig. 3*h*). Furthermore, when Kv1.2-containing K^+ channels were present, there was a significant increase in the percentage that located in paranodal regions (Fig. 3*i*).

To determine whether α II spectrin is also required at CNS nodes, we performed intravitreal injections of AAV-GFP or AAV-cre-GFP into *Sptan1^{fl/fl}* mice. Whereas immunostaining of optic nerves from mice injected with AAV-GFP showed intact nodal β IV spectrin and Nfasc staining (Fig. 4*a*), the nodes along axons of retinal ganglion cells transduced with AAV-cre-GFP

were dramatically disrupted (Fig. 4*a*). Quantification showed that nodes were frequently fragmented and had substantially reduced amounts of nodal proteins (Fig. 4*b*). Together, these observations demonstrate that α II spectrin is required for proper assembly and maintenance of nodal, paranodal, and juxtapanodal domains.

Large-diameter axons have a higher density of nodal α II spectrin

While determining the distribution of α II spectrin at and near nodes, we noticed that small nodes (small-diameter myelinated axons) had less nodal α II spectrin immunoreactivity than large nodes (large-diameter myelinated axons) (Fig. 5*a*). However, all nodes appeared to have similar amounts of β IV spectrin and NF186 immunoreactivity. To determine whether large nodes have a higher density of α II spectrin than small nodes, we triple-labeled nodes of Ranvier using antibodies against Nfasc, β IV spectrin, and α II spectrin. We then measured the fluorescence

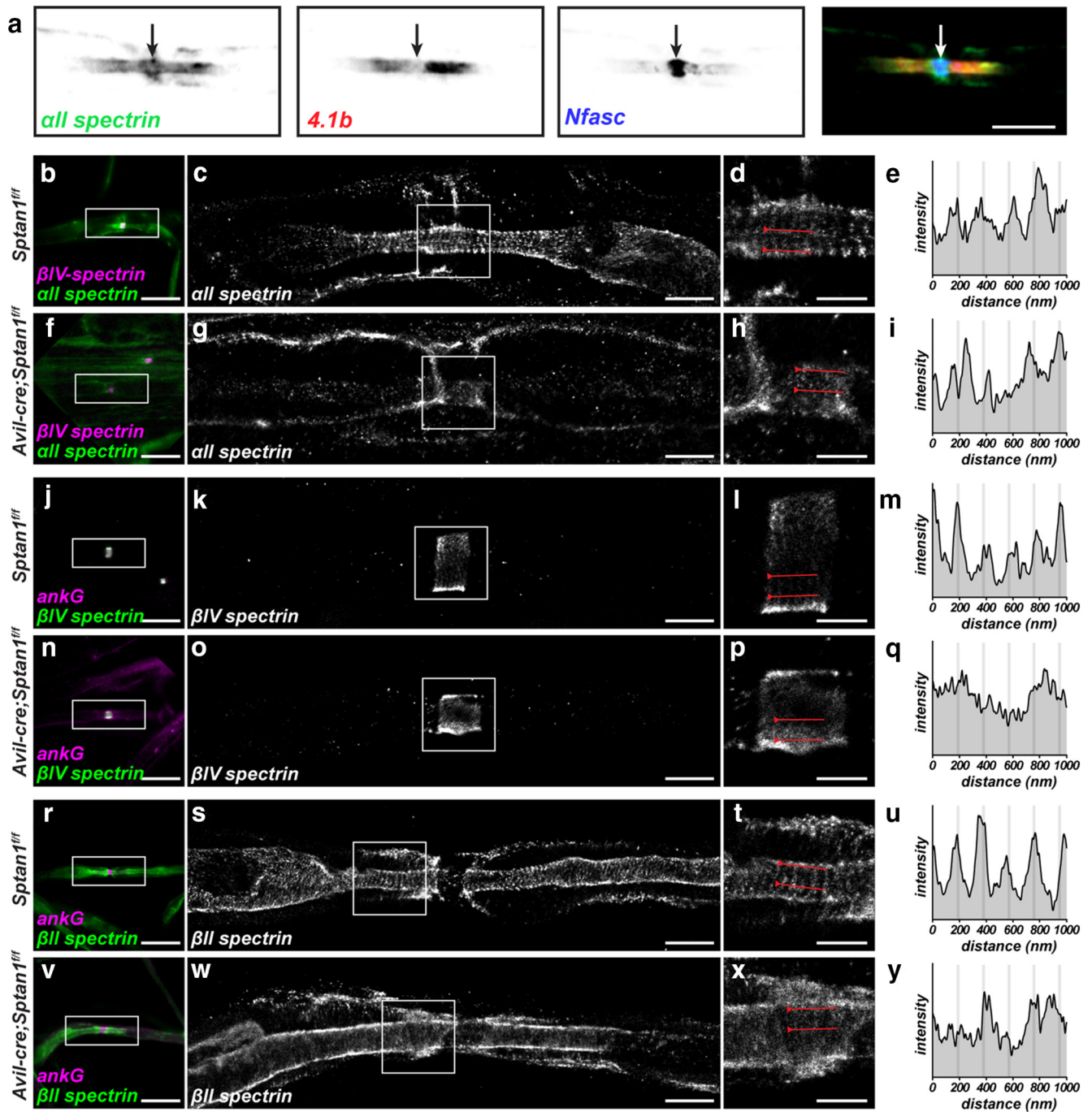


Figure 2. α II spectrin is enriched at nodes of Ranvier in large-diameter axons. **a**, Detergent-extracted adult sciatic nerve node of Ranvier labeled for α II spectrin (green), protein 4.1b (red), and Nfasc (blue). Arrow indicates the position of the node. Scale bar, 5 μ m. **b–y**, Teased dorsal root axons from 5-month-old *Sptan1^{fl/fl}* and *Avil-cre;Sptan1^{fl/fl}* mice. **b–i**, Conventional immunofluorescence (magenta represents β IV spectrin; green represents α II spectrin; **b, f**) and STORM imaging (α II spectrin; **c, d, g, h**) of control *Sptan1^{fl/fl}* (**b–d**) and α II spectrin-deficient *Avil-cre;Sptan1^{fl/fl}* (**f–h**) mouse dorsal roots. **c, g**, Boxes surround nodes and correspond to the STORM images shown in **d** and **h**, respectively. The regions between the lines in **d** and **h** were used to generate an α II spectrin intensity profile (**e, i**). Scale bars: **b, f**, 10 μ m; **c, g**, 2 μ m; **d, h**, 1 μ m. **j–q**, Conventional immunofluorescence (magenta represents ankG; green represents β IV spectrin; **j, n**) and STORM imaging (β IV spectrin; **k, l, o, p**) of control *Sptan1^{fl/fl}* (**j–l**) and α II spectrin-deficient *Avil-cre;Sptan1^{fl/fl}* (**n–p**) mouse dorsal roots. **k, o**, Boxes surround nodes and correspond to the STORM images shown in **l** and **p**, respectively. **l, p**, The regions between the lines were used to generate a β IV spectrin intensity profile (**m, q**). Scale bars: **j, n**, 10 μ m; **k, o**, 2 μ m; **l, p**, 1 μ m. **r–y**, Conventional immunofluorescence (magenta represents ankG; green represents β II spectrin; **r, v**) and STORM imaging (β II spectrin; **s, t, w, x**) of control *Sptan1^{fl/fl}* (**r–t**) and α II spectrin-deficient *Avil-cre;Sptan1^{fl/fl}* (**v–x**) mouse dorsal roots. **s, w**, Boxes are located in paranodal regions and correspond to the STORM images shown in **t** and **x**, respectively. **t, x**, The regions between the lines were used to generate a β II spectrin intensity profile (**u, y**). Scale bars: **r, v**, 10 μ m; **s, w**, 2 μ m; **t, x**, 1 μ m.

intensity of each spectrin at nodes and normalized it to the fluorescence intensity of its corresponding nodal Nfasc. We normalized the spectrin immunoreactivities to Nfasc because its nodal localization in the PNS can be independent of its interaction with the nodal cytoskeleton (Dzhashiashvili et al., 2007). Remarkably,

we found that, whereas the β IV spectrin/Nfasc ratio was constant across a wide range of nodal areas, smaller nodes had a significantly lower α II spectrin/Nfasc ratio (Fig. 5b). Thus, large nodes found along large-diameter axons have a higher density of nodal α II spectrin.

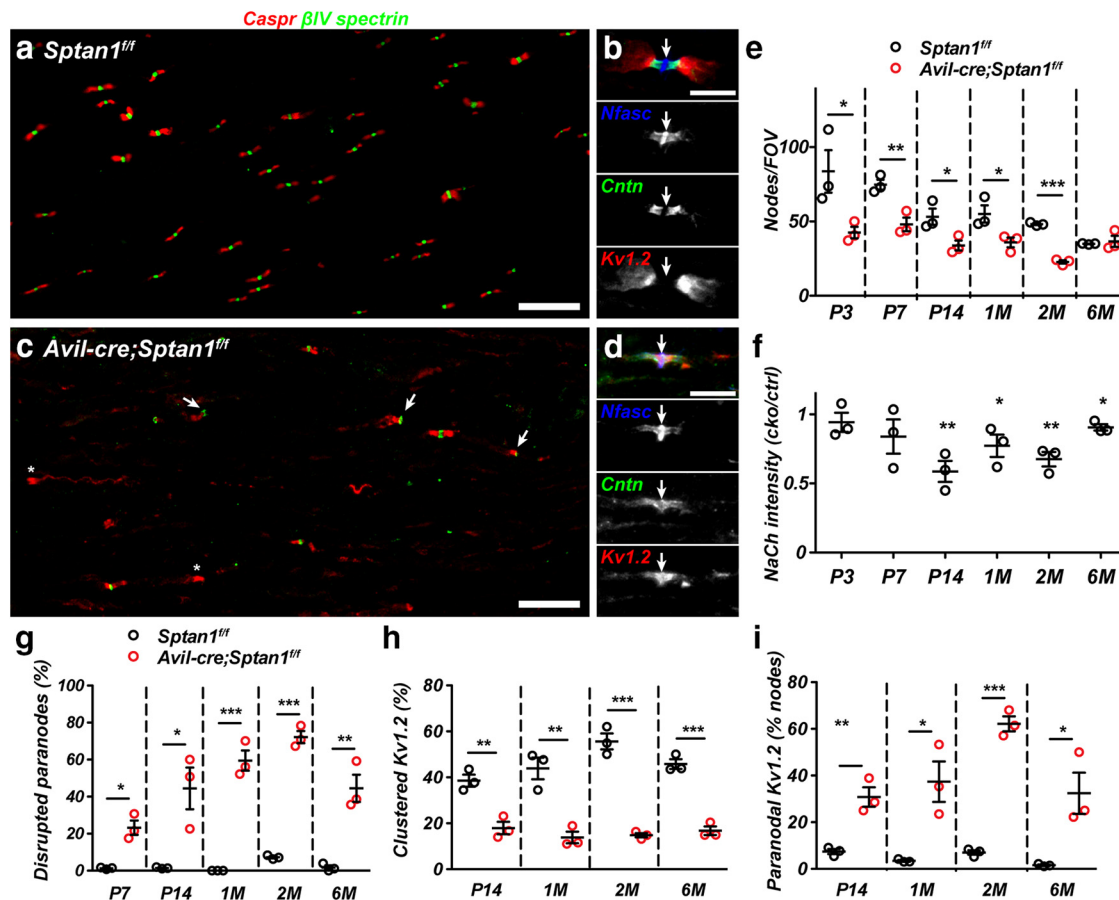


Figure 3. Nodes of Ranvier are disrupted in α II spectrin-deficient axons. **a**, Sections of dorsal roots from a 2-month-old *Sptan1^{f/f}* mouse were immunostained for Caspr (red) and β IV spectrin (green). Scale bar, 20 μ m. **b**, A dorsal root node of Ranvier from a 2-month-old *Sptan1^{f/f}* mouse immunostained for Nfasc (blue), contactin (Cntn) (green), and kv1.2 (red). Arrow indicates the node. Scale bar, 5 μ m. **c**, Sections of dorsal roots from a 2-month-old *Avil-cre;Sptan1^{f/f}* mouse were immunostained for Caspr (red) and β IV spectrin (green). Scale bar, 20 μ m. **d**, A dorsal root node of Ranvier from a 2-month-old *Avil-cre;Sptan1^{f/f}* mouse immunostained for Nfasc (blue), contactin (Cntn) (green), and kv1.2 (red). Arrow indicates the node. Scale bar, 5 μ m. **e**, The number of nodes per FOV, determined by β IV spectrin immunostaining in dorsal roots from *Sptan1^{f/f}* and *Avil-cre;Sptan1^{f/f}* mice. P3: $p = 0.0498$, $t_{(4)} = 2.781$; P7: $^{**}p = 0.0090$, $t_{(4)} = 4.750$; P14: $p = 0.0394$, $t_{(4)} = 3.015$; 1 month: $^{*}p = 0.0451$, $t_{(4)} = 2.878$; 2 months: $^{***}p = 3.6123E-05$, $t_{(4)} = 20.11$; 6 months: $p = 0.6720$, $t_{(4)} = 0.4560$. **f**, The intensity of Na⁺ channel (NaCh) immunostaining in dorsal roots from *Sptan1^{f/f}* and *Avil-cre;Sptan1^{f/f}* mice. The intensity was calculated as a ratio of the average nodal Na⁺ channel immunoreactivity in the *Avil-cre;Sptan1^{f/f}* mouse divided by the average nodal Na⁺ channel immunoreactivity in *Sptan1^{f/f}* mice. Each data point indicates a pair of matched *Sptan1^{f/f}* and *Avil-cre;Sptan1^{f/f}* mice that were immunostained and analyzed at the same time. P3: $p = 0.5311$, $t_{(4)} = 0.6848$; P7: $p = 0.2051$, $t_{(4)} = 1.512$; P14: $^{**}p = 0.0059$, $t_{(4)} = 5.345$; 1 month: $^{*}p = 0.0121$, $t_{(4)} = 4.352$; 2 months: $^{***}p = 0.0053$, $t_{(4)} = 5.496$; 6 months: $^{*}p = 0.0162$, $t_{(4)} = 3.995$. **g**, The percentage of disrupted paranodes indicated by aberrant Caspr immunostaining as a function of age. P7: $^{*}p = 0.0049$, $t_{(4)} = 5.622$; P14: $^{*}p = 0.0187$, $t_{(4)} = 3.822$; 1 month: $^{***}p = 0.0004$, $t_{(4)} = 10.91$; 2 months: $^{***}p = 4.10125E-05$, $t_{(4)} = 19.47$; 6 months: $^{**}p = 0.0046$, $t_{(4)} = 5.725$. **h**, The percentage of dorsal root nodes of Ranvier with flanking clustered juxtapanodal kv1.2-containing K⁺ channels as a function of age. P14: $^{***}p = 0.0054$, $t_{(4)} = 5.491$; 1 month: $^{***}p = 0.0049$, $t_{(4)} = 5.628$; 2 months: $^{***}p = 0.0003$, $t_{(4)} = 11.33$; 6 months: $^{***}p = 0.0005$, $t_{(4)} = 10.33$. **i**, The percentage of paranodes that also show Kv1.2 immunoreactivity. P14: $^{***}p = 0.0055$, $t_{(4)} = 5.447$; 1 month: $^{*}p = 0.0174$, $t_{(4)} = 3.913$; 2 months: $^{***}p = 7.61026E-05$, $t_{(4)} = 16.66$; 6 months: $^{*}p = 0.0252$, $t_{(4)} = 3.489$. **e–i**, $N = 3$ mice per genotype at each time point indicated.

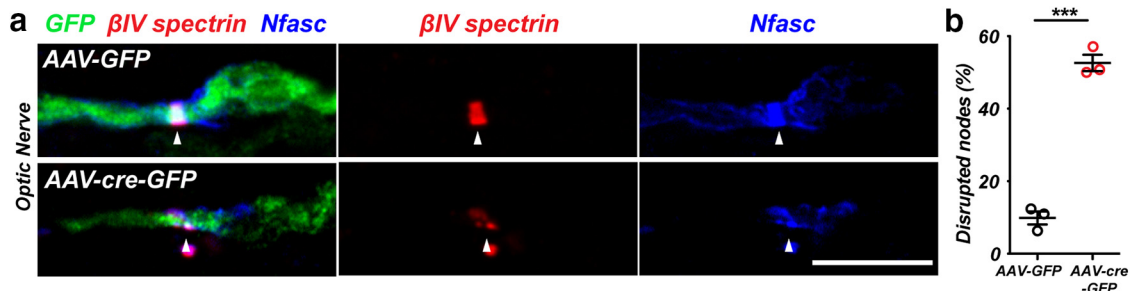


Figure 4. **a**, *Sptan1^{f/f}* mice were intravitreally injected with AAV-GFP (control) or AAV-cre-GFP (KO). One month later, optic nerves were immunostained for GFP (green), β IV spectrin (red), and Nfasc (blue). Arrowheads indicate the node. Scale bar, 5 μ m. **b**, The percentage of disrupted nodes in GFP⁺ axons. $N = 3$ mice for each indicated virus. $^{***}p = 0.0001$, $t_{(4)} = 14.71$.

Loss of α II spectrin causes degeneration of large-diameter, myelinated axons

How can sensory neuron-specific loss of α II spectrin cause ataxia and motor dysfunction but not impair nociception? Although

nodes are clearly disrupted, another explanation is that large-diameter, myelinated axons responsible for proprioception degenerate because of a greater dependence on α II spectrin, but unmyelinated axons remain intact. This possibility is consistent

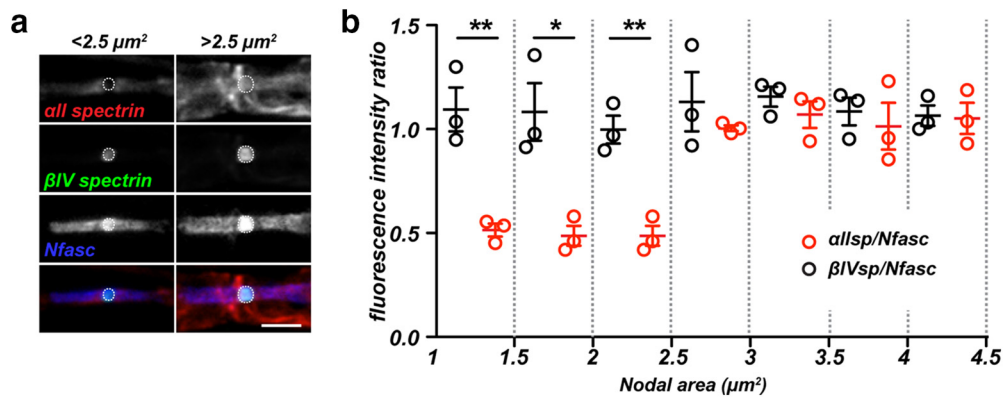


Figure 5. *a*, Immunolabeling of small ($<2.5 \mu\text{m}^2$) and large ($>2.5 \mu\text{m}^2$) nodes of Ranvier for α II spectrin (red), β IV spectrin (green), and Nfasc (blue). Fluorescence intensities were measured inside of the dotted circles and used to calculate the fluorescence intensity ratios shown in *b*. Scale bar, $10 \mu\text{m}$. *b*, The fluorescence intensity ratio of α II spectrin/Nfasc (red) and β IV spectrin/Nfasc (black) as a function of nodal area. $N = 3$ mice. Data are mean \pm SEM. 1–1.5: ** $p = 0.0061$, $t_{(4)} = 5.285$; 1.5–2: * $p = 0.0152$, $t_{(4)} = 4.071$; 2–2.5: ** $p = 0.0034$, $t_{(4)} = 6.212$; 2.5–3: $p = 0.4245$, $t_{(4)} = 0.8884$; 3–3.5: $p = 0.3394$, $t_{(4)} = 1.084$; 3.5–4: $p = 0.6175$, $t_{(4)} = 0.5406$; 4–4.5: $p = 0.8959$, $t_{(4)} = 0.1394$.

with the observation that the nodes of large-diameter axons have more α II spectrin (Fig. 5). To determine whether loss of α II spectrin also causes axon degeneration, we examined toluidine blue-stained cross sections of 3-month-old dorsal roots. We found that *Sptan1^{fl/fl}* and *Avil-cre;Sptan1^{fl/fl}* mice had dramatic differences in the number of large-diameter axons and that there was obvious degeneration of the largest axons (Fig. 6*a*, asterisks). We then used electron microscopy to examine the ultrastructure of sensory axons in neonatal, juvenile, and adult mice. As early as 1 week after birth, we saw axon degeneration in *Avil-cre;Sptan1^{fl/fl}* dorsal roots, and this became more prominent with increasing age (Fig. 6*b*, arrows). Degenerating axons often had thin myelin profiles containing the remnants of axons (Fig. 6*b*, arrows), whereas others were filled with vesicles and debris (Fig. 6*b*, 1 and 3 months, asterisks). Although there was no difference in axon diameter at P7 and P14 (Fig. 6*c*), we measured a significant increase in the g-ratio (ratio of the inner axon diameter to the outer diameter of the myelin sheath) at these time points, indicating thinner myelin (Fig. 6*d*). This observation, together with the fewer nodes of Ranvier observed at P3 (Fig. 3*e*; before any axon degeneration), may suggest delayed myelination of axons lacking α II spectrin. Axon diameter gradually increased with age in *Sptan1^{fl/fl}* mice but remained unchanged in *Avil-cre;Sptan1^{fl/fl}* mice. Interestingly, with increasing age, the g-ratio decreased below that of control myelinated axons (Fig. 6*d*), consistent with the fact that remaining axons are smaller, but heavily myelinated (Fig. 6*b*). Plotting g-ratio as a function of axon diameter in 3-month-old *Avil-cre;Sptan1^{fl/fl}* mice clearly showed the loss of large-diameter axons (Fig. 6*e*). Together, these results suggest that loss of α II spectrin results in preferential degeneration of large-diameter myelinated axons.

To further define the population of sensory neurons whose axons degenerate in response to loss of α II spectrin, we immunostained DRGs using antibodies against ATF3, a transcription factor induced in response to axon injury (Tsujino et al., 2000). We found many ATF3⁺ neurons in *Avil-cre;Sptan1^{fl/fl}* DRG, but ATF3 labeling was not detected in *Sptan1^{fl/fl}* mice (Fig. 7*a*). However, we did not detect any TUNEL staining in DRG at 1 month (data not shown), suggesting that, despite axon degeneration, neuronal cell bodies remain. The diameter of DRG neuron cell bodies correlates well with both function and axon diameter; small-diameter DRG neurons have small unmyelinated axons, whereas large-diameter neurons have large myelinated axons (Rasband et al.,

2001). To determine whether α II spectrin-deficient large-diameter DRG neurons are preferentially ATF3⁺ compared with α II spectrin-deficient small-diameter neurons, we measured the diameters of DRG neurons and the diameters of ATF3⁺ DRG neurons in P10, P14, and 1-, 2-, and 6-month-old *Avil-cre;Sptan1^{fl/fl}* mice. We found that, at all time points, the median diameters of ATF3⁺ neurons were significantly larger than the median diameters of all neurons at the equivalent time point (Fig. 7*b*). Furthermore, the range of the diameters, as indicated in the box-and-whisker plots, confirmed that the ATF3⁺ neurons were always the largest neurons, but the smallest diameter neurons were never ATF3⁺. We also determined the proportion of ATF3⁺ DRG neurons and found that it increased gradually over the first month and plateaued at \sim 30% (Fig. 7*c*).

Because large-diameter DRG neurons were preferentially ATF3⁺, we next examined whether the sensory endings of small-diameter DRG neurons (nociceptors) or large-diameter A α and A β DRG neurons (proprioceptors and mechanoreceptors) are disrupted in the absence of α II spectrin. The cornea is densely innervated by small-diameter axons (Fig. 8*a*) and has been used to quantitatively measure small-fiber neuropathy. Indeed, changes in corneal small-fiber density correlate well with nerve fiber density measurements from skin biopsies of patients with peripheral neuropathy (Malik et al., 2003; Tavakoli et al., 2010; Gao et al., 2016). To examine their innervation, we labeled corneas from *Sptan1^{fl/fl}* and *Avil-cre;Sptan1^{fl/fl}* mice using antibodies against β III tubulin (Tuj1; Fig. 8*b*). Consistent with the observed normal performance on the tail flick assay (Fig. 1*e*), we found no difference in the extent of α II spectrin-deficient small-fiber innervation of the cornea compared with controls (Fig. 8*c*).

To determine whether large-diameter, mechanosensory nerve endings are affected by loss of α II spectrin, we genetically labeled control and α II spectrin-deficient sensory neurons using ChR2-EYFP (ChR2-EYFP efficiently labels the cell membrane). Mechanosensory neurons innervate hair follicles in the skin to form mechanosensory end organs (Fig. 8*a*). These mechanosensory end organs consist of a circumferential ring of axons and lanceolate endings that run parallel to the hair follicle (Li and Ginty, 2014). Immunostaining of mechanosensory organs in *Avil-cre;Sptan1^{fl/fl};ChR2-EYFP* mice showed that, although the circumferential ring of axons remained intact, the lanceolate endings were lost (Fig. 8*d,e*). Proprioceptive nerve endings form muscle spindle stretch-sensitive nerve endings that spiral around intrafusal

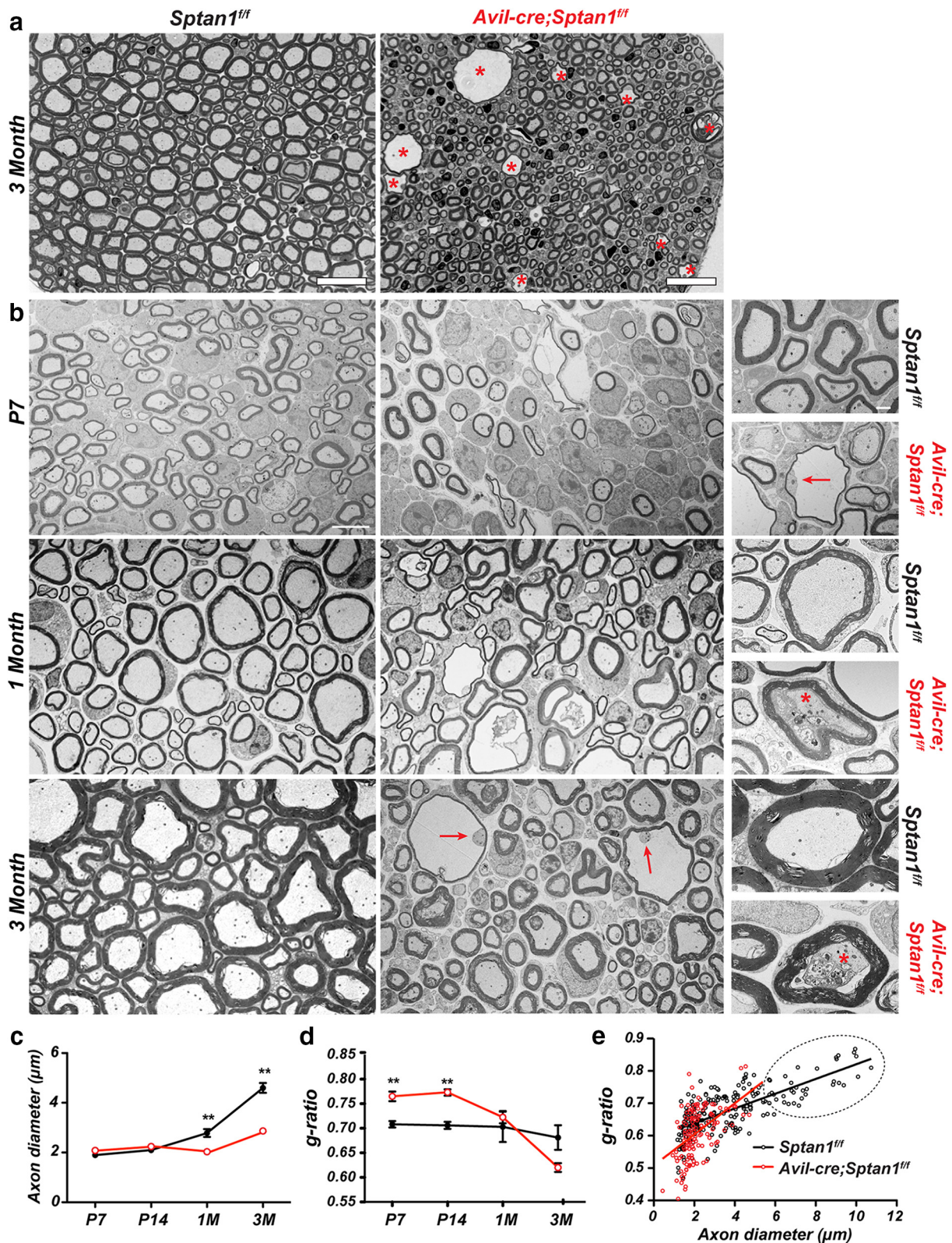


Figure 6. Large-diameter axons lacking α II spectrin degenerate. **a**, Toluidine blue-stained dorsal root cross sections from 3-month-old *Sptan1^{fl/fl}* and *Avil-cre; Sptan1^{fl/fl}* mice. Asterisks indicate degenerating axons. Scale bar, 20 μ m. **b**, TEM images of dorsal root cross sections from *Sptan1^{fl/fl}* and *Avil-cre; Sptan1^{fl/fl}* mice at P7, 1 month, and 3 months of age. Scale bar, 4 μ m. Right panels, Higher-magnification images of individual axons. Arrows indicate the degenerating axons. Asterisks indicate degenerating axons filled with vesicles and debris. Scale bar, 1 μ m. **c**, Axon diameters at the different ages shown for *Sptan1^{fl/fl}* and *Avil-cre; Sptan1^{fl/fl}* mice. $N = 3$ mice per genotype at each time point indicated. Data are mean \pm SEM. P7: $p = 0.0563$, $t_{(4)} = 2.662$; P14: $p = 0.2798$, $t_{(4)} = 1.249$; 1 month: $**p = 0.0093$, $t_{(4)} = 4.708$; 3 month: $**p = 0.0014$, $t_{(4)} = 7.947$. **d**, g-ratios at each time point indicated for *Sptan1^{fl/fl}* and *Avil-cre; Sptan1^{fl/fl}* mice. $N = 3$ mice per genotype at each time point indicated. Data are mean \pm SEM. P7: $**p = 0.0058$, $t_{(4)} = 5.376$; P14: $**p = 0.0010$, $t_{(4)} = 8.573$; 1 month: $p = 0.6481$, $t_{(4)} = 0.4927$; 3 month: $p = 0.0856$, $t_{(4)} = 2.271$. **e**, Scatterplot of g-ratio versus axon diameter from dorsal roots of 3-month-old *Sptan1^{fl/fl}* and *Avil-cre; Sptan1^{fl/fl}* mice. Dotted area represents *Avil-cre; Sptan1^{fl/fl}* mice devoid of large-diameter axons. *Sptan1^{fl/fl}*, $n = 188$ axons; *Avil-cre; Sptan1^{fl/fl}*, $n = 164$ axons.

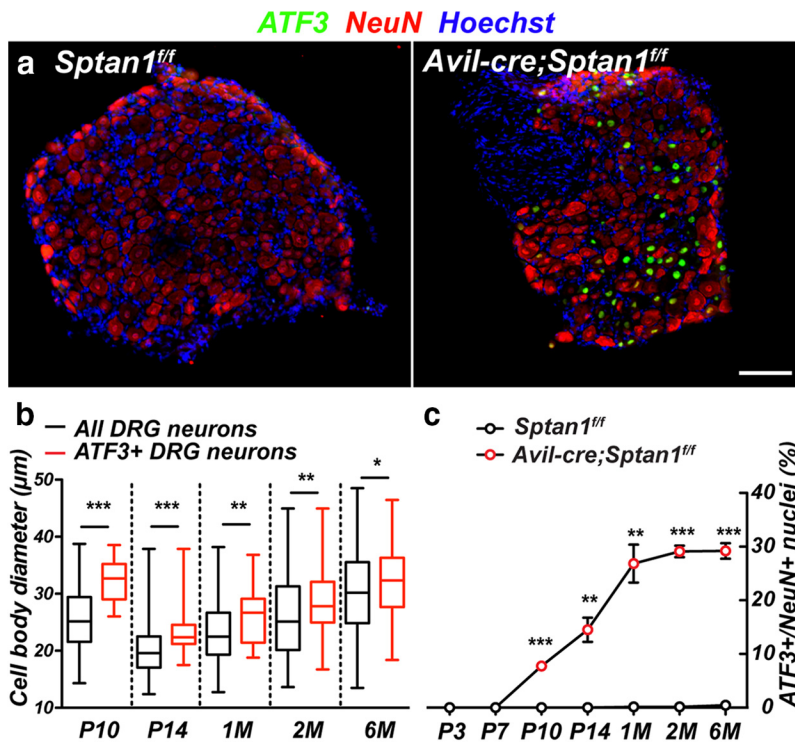


Figure 7. Large-diameter neurons lacking α II spectrin are labeled with injury markers. **a**, DRGs from 1-month-old control *Sptan1^{f/f}* and α II spectrin-deficient *Avil-cre; Sptan1^{f/f}* mice were immunostained using antibodies against ATF3 (green), NeuN (red), and Hoechst (blue). ATF3 was used as an injury marker. Scale bar, 50 μ m. **b**, DRG neuron diameter at the indicated time points. $N = 9, 12, 18, 11,$ and 16 DRGs at P10, P14, 1 month, 2 months, and 6 months, respectively. Data are presented as box-and-whisker plots. P10: *** $p = 0.0005$, $t_{(145)} = 3.559$; P14: *** $p = 0.0006$, $t_{(145)} = 3.494$; 1 month: ** $p = 0.0018$, $t_{(242)} = 3.159$; 2 months: ** $p = 0.0086$, $t_{(200)} = 2.653$; 6 months: * $p = 0.0320$, $t_{(284)} = 2.155$. **c**, Quantification of ATF3⁺ neurons in DRGs across different stages. For *Sptan1^{f/f}* mice: $N = 11, 10, 9, 8, 14, 10,$ and 17 DRGs at P3, P7, P10, P14, 1 month, 2 months, and 6 months, respectively. For *Avil-cre; Sptan1^{f/f}* mice: $N = 11, 9, 9, 12, 18, 11,$ and 16 DRGs at P3, P7, P10, P14, 1 month, 2 months, and 6 months, respectively. P7: $p = 0.3739$, $t_{(4)} = 1$; P10: *** $p = 0.0002$, $t_{(4)} = 12.8552$; P14: ** $p = 0.0029$, $t_{(4)} = 6.4514$; 1 month: ** $p = 0.0016$, $t_{(4)} = 7.558$; 2 months: *** $p = 1.08206E-05$, $t_{(4)} = 27.23$; 6 months: *** $p = 3.76902E-05$, $t_{(4)} = 19.89$.

fibers in skeletal muscle (Fig. 8*a*). These muscle spindles were identified by costaining for S46 to label intrafusal fibers, and EYFP to label sensory neurons. Whereas $\sim 75\%$ of intrafusal fibers were associated with a spiral nerve terminal, α II spectrin-deficient proprioceptive muscle spindles were either completely absent or failed to spiral around intrafusal fibers (Fig. 8*f,g*). Together, these observations demonstrate that loss of α II spectrin causes preferential degeneration of large-diameter, myelinated axons responsible for proprioception and mechanoreception.

Discussion

Hammarlund et al. (2007) previously reported the striking result that β spectrin-deficient *Caenorhabditis elegans* had fragile axons that break due to mechanical forces experienced by movement. However, paralyzing β spectrin-deficient nematodes inhibited the breakage of axons. These results support the notion that spectrin cytoskeletons help protect axons from mechanical forces that would otherwise cause axon degeneration. Whether β spectrins play a similar function in vertebrate neurons is unknown and difficult to determine because vertebrate neurons may contain as many as four different β subunits (β I– β IV); and in some contexts, these β spectrins can substitute for one another (Ho et al., 2014). However, deletion of α II spectrin dramatically reduces the overall amount of β spectrins (Huang et al., 2017), which may be due to rapid degradation and proteolysis when not incorporated

and stabilized in the submembranous cytoskeleton. Surprisingly, mice with α II spectrin-deficient peripheral sensory neurons showed only degenerating large-diameter myelinated axons; small-diameter axons remained intact. In contrast, loss of α II spectrin in the CNS causes widespread axon degeneration (Huang et al., 2017). Why are large-diameter PNS sensory axons preferentially affected by loss of α II spectrin, and why is axon degeneration more pervasive in mice lacking CNS α II spectrin? The difference may be explained by the unique morphologies and functions of these cells. Whereas DRG neurons are pseudo-unipolar, lack dendrites, and their function does not depend on the AIS, most CNS neurons are multipolar and their proper function requires intact AIS (Ho et al., 2014). Disruption or loss of the AIS in CNS neurons causes axons to acquire the structural and molecular characteristics of dendrites (Hedstrom et al., 2008; Sobotzik et al., 2009). We showed that loss of α II spectrin disrupts AIS and impairs its assembly (Galiano et al., 2012). Future studies may help determine whether loss of α II spectrin contributes to axon degeneration by altering polarized trafficking of somatodendritic or axonal cargoes. Thus, using mice with loss of CNS α II spectrin, it is not possible to uncouple the contribution of the disrupted AIS to axon degeneration, from the contribution of disrupted nodes of Ranvier or disrupted axonal cytoskeleton in non-nodal regions. Our use of *Avil-cre; Sptan1^{f/f}* mice is central to answering

questions regarding the role of the periodic, spectrin-dependent cytoskeleton in axons.

The preferential degeneration of large-diameter myelinated axons is a surprising result because current models for spectrin function suggest that the periodic axonal spectrin cytoskeleton provides structural support to resist mechanical forces (Xu et al., 2013). Because small-diameter axons did not degenerate for at least 6 months (the period we studied), we conclude that, unlike *C. elegans*, vertebrate axons may have additional spectrin-independent mechanisms to support their integrity. Similarly, axon degeneration was not reported in zebrafish mutants lacking α II spectrin (Voas et al., 2007), although larval lethality precluded a longer analysis. Other mechanisms stabilizing vertebrate axons may include microtubule cytoskeletons that in worms have been reported to contribute to axon stability (Krieg et al., 2017). However, these additional mechanisms cannot support large-diameter axons. Alternatively, small-diameter axons may be less susceptible to mechanical trauma due to their smaller mass and volumes.

Nodes of Ranvier: the axon's Achilles heel

Could disruption of the nodal and/or paranodal cytoskeletons account for the degeneration of large-diameter axons? There are many mutant mice with disrupted paranodes (e.g., Caspr-null, contactin-null) that do not show axon degeneration (Berglund

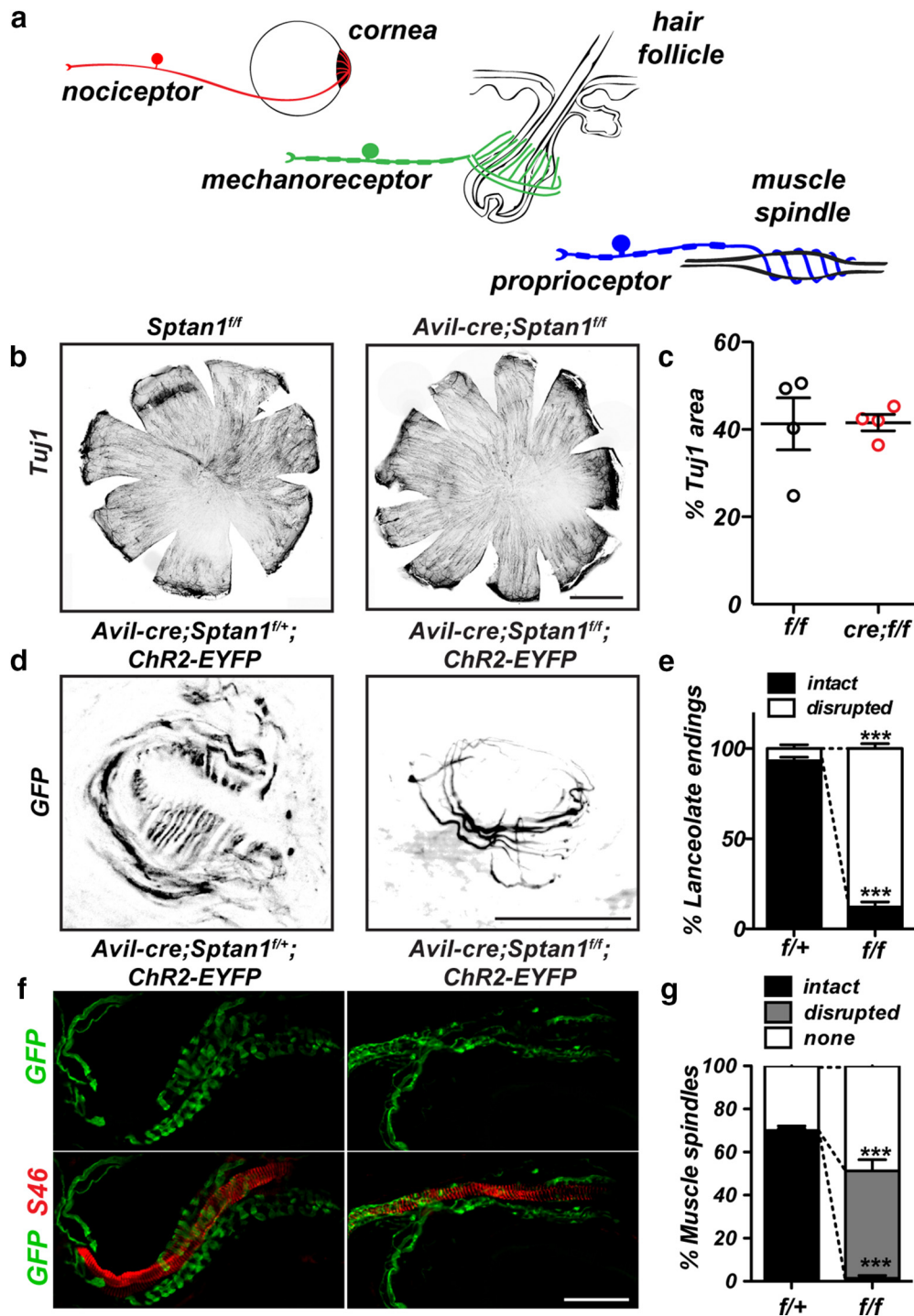


Figure 8. *a*, Diagram illustrating (1) innervation of cornea by small-diameter axon nociceptors, (2) the lanceolate endings and large-diameter axons of mechanoreceptors surrounding hair cells, and (3) the stretch-sensitive large-diameter axons of proprioceptors that form a muscle spindle as the axon spirals around intrafusal muscle fibers. *b*, Corneas from 6-week-old control *Sptan1^{f/f}* and α II spectrin-deficient *Avil-cre; Sptan1^{f/f}* mice immunostained against Tuj1. Scale bar, 1 mm. *c*, The percentage of cornea that is Tuj1⁺. *N* = 4 corneas. Data are mean \pm SEM. *d*, Hair follicles in skin from 2-month-old control *Avil-cre; Sptan1^{f/f}; Chr2-EYFP* and sensory neuron-specific α II spectrin-deficient *Avil-cre; Sptan1^{f/f}; Chr2-EYFP* mice were immunostained against GFP. Scale bar, 20 μ m. *e*, The percentage of hair follicles with intact lanceolate endings in *Avil-cre; Sptan1^{f/f}; Chr2-EYFP* (*f/f*) and *Avil-cre; Sptan1^{f/f}; Chr2-EYFP* (*f/f*) mice. *N* = 3, 2-month-old animals. Data are mean \pm SEM. Intact: ****p* = 1.83392E-05, *t*₍₄₎ = 23.85; disrupted: ****p* = 1.94369E-05, *t*₍₄₎ = 23.50. *f*, Gastrocnemius muscles from 2-month-old control *Avil-cre; Sptan1^{f/f}; Chr2-EYFP* and sensory neuron-specific α II spectrin-deficient *Avil-cre; Sptan1^{f/f}; Chr2-EYFP* mice were immunostained using antibodies against GFP and S46. Muscle spindles coil around S46-labeled intrafusal muscle fibers. Scale bar, 50 μ m. *g*, The percentage of intact and disrupted muscle spindles in *Avil-cre; Sptan1^{f/f}; Chr2-EYFP* (*f/f*) and *Avil-cre; Sptan1^{f/f}; Chr2-EYFP* (*f/f*) mice. *N* = 3, 2-month-old animals. Intact: ****p* = 5.2687E-05, *t*₍₄₎ = 18.28; disrupted: ****p* = 0.0007, *t*₍₄₎ = 9.353; none: *p* = 0.0544, *t*₍₄₎ = 2.678.

et al., 1999; Bhat et al., 2001; Pillai et al., 2009). Even loss of β II spectrin and disruption of the paranodal spectrin cytoskeleton in both large- and small-diameter axons do not cause axon degeneration (Zhang et al., 2013; Amor et al., 2017). Thus, disruption

of the paranodal cytoskeleton cannot account for the degeneration. Although node disruption was common among all fiber types in *Avil-cre; Sptan1^{f/f}* mice, it did not presage axon degeneration because small-diameter myelinated axons did not degener-

ate. We observed disruption of node assembly already at P3, but we did not see ATF3⁺ DRG until P10, suggesting that node disruption and axon degeneration are independent events. Instead, we found a striking (~50%) increase in the density of α II spectrin as the size of the node (a surrogate measurement for axon diameter) increased. The internodal regions of large-diameter axons are ensheathed by many layers of compact myelin that could also provide mechanical support against stretch, compression, and torsion. However, we speculate that nodes of Ranvier (gaps in the myelin sheath) along large-diameter axons are particularly susceptible to injury or mechanical disruption due to the larger mass and volume of the axons they support, and that an increased density of α II spectrin may stabilize and protect these nodes. Here, we only examined peripheral sensory axons, but future studies of large-diameter motor axons in peripheral nerves may show similar degeneration and directly test this idea. Alternatively, deletion of α II spectrin in adult mice, after nodes, myelin, and large-diameter sensory axons have formed, may provide additional insight into α II spectrin's function in maintaining large-diameter axon integrity.

Because α and β spectrins form tetramers (2 α and 2 β subunits), it is not clear how more α II spectrin stabilizes a node, or how more α II spectrin is recruited to a node. Nevertheless, our results have important implications for nervous system development, injury, and disease. Proteolysis of α II spectrin is a common sequela of ischemia, trauma, or any event resulting in elevated intracellular calcium (Czogalla and Sikorski, 2005). We speculate that more α II spectrin in large nodes may provide a reserve that can be incorporated into the nodal submembranous cytoskeleton or a pool that functions as a buffer for spectrin degradation. Thus, protection of α II spectrin may be an important component of future neuroprotective therapies.

References

- Amor V, Zhang C, Vainshtein A, Zhang A, Zollinger DR, Eshed-Eisenbach Y, Brophy PJ, Rasband MN, Peles E (2017) The paranodal cytoskeleton clusters Na⁺ channels at nodes of Ranvier. *eLife* 6:e21392. [CrossRef Medline](#)
- Bennett V, Lorenzo DN (2013) Spectrin- and ankyrin-based membrane domains and the evolution of vertebrates. *Curr Top Membr* 72:1–37. [CrossRef Medline](#)
- Berghs S, Agujaro D, Dirx R Jr, Maksimova E, Stabach P, Hermel JM, Zhang JP, Philbrick W, Slepnev V, Ort T, Solimena M (2000) betaIV spectrin, a new spectrin localized at axon initial segments and nodes of Ranvier in the central and peripheral nervous system. *J Cell Biol* 151:985–1002. [CrossRef Medline](#)
- Berglund EO, Murai KK, Fredette B, Sekerková G, Marturano B, Weber L, Mugnaini E, Ranscht B (1999) Ataxia and abnormal cerebellar microorganization in mice with ablated contactin gene expression. *Neuron* 24:739–750. [CrossRef Medline](#)
- Bhat MA, Rios JC, Lu Y, Garcia-Fresco GP, Ching W, St Martin M, Li J, Einheber S, Chesler M, Rosenbluth J, Salzer JL, Bellen HJ (2001) Axon-glia interactions and the domain organization of myelinated axons requires neuexin IV/Caspr/Paranodin. *Neuron* 30:369–383. [CrossRef Medline](#)
- Chang KJ, Rasband MN (2013) Excitable domains of myelinated nerves: axon initial segments and nodes of Ranvier. *Curr Top Membr* 72:159–192. [CrossRef Medline](#)
- Czogalla A, Sikorski AF (2005) Spectrin and calpain: a 'target' and a 'sniper' in the pathology of neuronal cells. *Cell Mol Life Sci* 62:1913–1924. [CrossRef Medline](#)
- D'Este E, Kamin D, Balzarotti F, Hell SW (2017) Ultrastructural anatomy of nodes of Ranvier in the peripheral nervous system as revealed by STED microscopy. *Proc Natl Acad Sci U S A* 114:E191–E199. [CrossRef Medline](#)
- Dzhashiashvili Y, Zhang Y, Galinska J, Lam I, Grumet M, Salzer JL (2007) Nodes of Ranvier and axon initial segments are ankyrin G-dependent domains that assemble by distinct mechanisms. *J Cell Biol* 177:857–870. [CrossRef Medline](#)
- Galiano MR, Jha S, Ho TS, Zhang C, Ogawa Y, Chang KJ, Stankewich MC, Mohler PJ, Rasband MN (2012) A distal axonal cytoskeleton forms an intra-axonal boundary that controls axon initial segment assembly. *Cell* 149:1125–1139. [CrossRef Medline](#)
- Gao N, Yan C, Lee P, Sun H, Yu FS (2016) Dendritic cell dysfunction and diabetic sensory neuropathy in the cornea. *J Clin Invest* 126:1998–2011. [CrossRef Medline](#)
- Garcia-Fresco GP, Sousa AD, Pillai AM, Moy SS, Crawley JN, Tessarollo L, Dupree JL, Bhat MA (2006) Disruption of axo-glia junctions causes cytoskeletal disorganization and degeneration of Purkinje neuron axons. *Proc Natl Acad Sci U S A* 103:5137–5142. [CrossRef Medline](#)
- Hammarlund M, Jorgensen EM, Bastiani MJ (2007) Axons break in animals lacking beta-spectrin. *J Cell Biol* 176:269–275. [CrossRef Medline](#)
- Hasegawa H, Abbott S, Han BX, Qi Y, Wang F (2007) Analyzing somatosensory axon projections with the sensory neuron-specific Advillin gene. *J Neurosci* 27:14404–14414. [CrossRef Medline](#)
- Hedstrom KL, Ogawa Y, Rasband MN (2008) AnkyrinG is required for maintenance of the axon initial segment and neuronal polarity. *J Cell Biol* 183:635–640. [CrossRef Medline](#)
- Ho TS, Zollinger DR, Chang KJ, Xu M, Cooper EC, Stankewich MC, Bennett V, Rasband MN (2014) A hierarchy of ankyrin-spectrin complexes clusters sodium channels at nodes of Ranvier. *Nat Neurosci* 17:1664–1672. [CrossRef Medline](#)
- Huang CY, Zhang C, Ho TS, Oses-Prieto J, Burlingame AL, Lalonde J, Noebels JL, Leterrier C, Rasband MN (2017) α II spectrin forms a periodic cytoskeleton at the AIS and is required for nervous system function.
- Krieg M, Stühmer J, Cueva JG, Fetter R, Spilker K, Cremers D, Shen K, Dunn AR, Goodman MB (2017) Genetic defects in beta-spectrin and tau sensitize *C. elegans* axons to movement-induced damage via torque-tension coupling. *eLife* 6:e20172. [CrossRef Medline](#)
- Leterrier C, Potier J, Caillol G, Debarnot C, Rueda Boroni F, Dargent B (2015) Nanoscale architecture of the axon initial segment reveals an organized and robust scaffold. *Cell Rep* 13:2781–2793. [CrossRef Medline](#)
- Li L, Ginty DD (2014) The structure and organization of lanceolate mechanosensory complexes at mouse hair follicles. *eLife* 3:e01901. [CrossRef Medline](#)
- Malik RA, Kallinikos P, Abbott CA, van Schie CH, Morgan P, Efron N, Boulton AJ (2003) Corneal confocal microscopy: a non-invasive surrogate of nerve fibre damage and repair in diabetic patients. *Diabetologia* 46:683–688. [CrossRef Medline](#)
- Ogawa Y, Schafer DP, Horresh I, Bar V, Hales K, Yang Y, Susuki K, Peles E, Stankewich MC, Rasband MN (2006) Spectrins and ankyrinB constitute a specialized paranodal cytoskeleton. *J Neurosci* 26:5230–5239. [CrossRef Medline](#)
- Pillai AM, Thaxton C, Pribisko AL, Cheng JG, Dupree JL, Bhat MA (2009) Spatiotemporal ablation of myelinating glia-specific neurofascin (Nfasc NF155) in mice reveals gradual loss of paranodal axoglial junctions and concomitant disorganization of axonal domains. *J Neurosci Res* 87:1773–1793. [CrossRef Medline](#)
- Poliak S, Gollan L, Salomon D, Berglund EO, Ohara R, Ranscht B, Peles E (2001) Localization of Caspr2 in myelinated nerves depends on axon-glia interactions and the generation of barriers along the axon. *J Neurosci* 21:7568–7575. [Medline](#)
- Rasband MN (2010) The axon initial segment and the maintenance of neuronal polarity. *Nat Rev Neurosci* 11:552–562. [CrossRef Medline](#)
- Rasband MN, Park EW, Vanderah TW, Lai J, Porreca F, Trimmer JS (2001) Distinct potassium channels on pain-sensing neurons. *Proc Natl Acad Sci U S A* 98:13373–13378. [CrossRef Medline](#)
- Schafer DP, Jha S, Liu F, Akella T, McCullough LD, Rasband MN (2009) Disruption of the axon initial segment cytoskeleton is a new mechanism for neuronal injury. *J Neurosci* 29:13242–13254. [CrossRef Medline](#)
- Siman R, Baudry M, Lynch G (1984) Brain fodrin: substrate for calpain I, an endogenous calcium-activated protease. *Proc Natl Acad Sci U S A* 81:3572–3576. [CrossRef Medline](#)
- Sobotzik JM, Sie JM, Politi C, Del Turco D, Bennett V, Deller T, Schultz C (2009) AnkyrinG is required to maintain axo-dendritic polarity in vivo. *Proc Natl Acad Sci U S A* 106:17564–17569. [CrossRef Medline](#)
- Stankewich MC, Cianci CD, Stabach PR, Ji L, Nath A, Morrow JS (2011) Cell organization, growth, and neural and cardiac development require alphaII-spectrin. *J Cell Sci* 124:3956–3966. [CrossRef Medline](#)
- Susuki K, Chang KJ, Zollinger DR, Liu Y, Ogawa Y, Eshed-Eisenbach Y, Dours-Zimmermann MT, Oses-Prieto JA, Burlingame AL, Seidenbecher

- CI, Zimmermann DR, Oohashi T, Peles E, Rasband MN (2013) Three mechanisms assemble central nervous system nodes of Ranvier. *Neuron* 78:469–482. [CrossRef Medline](#)
- Tavakoli M, Marshall A, Pitceathly R, Fadavi H, Gow D, Roberts ME, Efron N, Boulton AJ, Malik RA (2010) Corneal confocal microscopy: a novel means to detect nerve fibre damage in idiopathic small fibre neuropathy. *Exp Neurol* 223:245–250. [CrossRef Medline](#)
- Tsujino H, Kondo E, Fukuoka T, Dai Y, Tokunaga A, Miki K, Yonenobu K, Ochi T, Noguchi K (2000) Activating transcription factor 3 (ATF3) induction by axotomy in sensory and motoneurons: a novel neuronal marker of nerve injury. *Mol Cell Neurosci* 15:170–182. [CrossRef Medline](#)
- Voas MG, Lyons DA, Naylor SG, Arana N, Rasband MN, Talbot WS (2007) α II-spectrin is essential for assembly of the nodes of Ranvier in myelinated axons. *Curr Biol* 17:562–568. [CrossRef Medline](#)
- Xu K, Zhong G, Zhuang X (2013) Actin, spectrin, and associated proteins form a periodic cytoskeletal structure in axons. *Science* 339:30495–30501. [CrossRef Medline](#)
- Yang Y, Ogawa Y, Hedstrom KL, Rasband MN (2007) β IV spectrin is recruited to axon initial segments and nodes of Ranvier by ankyrinG. *J Cell Biol* 176:509–519. [CrossRef Medline](#)
- Zhang C, Susuki K, Zollinger DR, Dupree JL, Rasband MN (2013) Membrane domain organization of myelinated axons requires betaII spectrin. *J Cell Biol* 203:437–443. [CrossRef Medline](#)
- Zhang Y, Chen K, Sloan SA, Bennett ML, Scholze AR, O’Keefe S, Phatnani HP, Guarnieri P, Caneda C, Ruderisch N, Deng S, Liddelow SA, Zhang C, Daneman R, Maniatis T, Barres BA, Wu JQ (2014) An RNA-sequencing transcriptome and splicing database of glia, neurons, and vascular cells of the cerebral cortex. *J Neurosci* 34:11929–11947. [CrossRef Medline](#)